

A single-band model with enhanced pairing from DMRG-based downfolding of the three-band Hubbard model

Shengtao Jiang (蒋晟韬)^{1,*} Douglas J. Scalapino,² and Steven R. White¹

¹*Department of Physics and Astronomy, University of California, Irvine, California 92697, USA*

²*Department of Physics, University of California, Santa Barbara, California 93106, USA*

(Dated: March 23, 2023)

Typical Wannier-function downfolding starts with a mean-field or density functional set of bands to construct the Wannier functions. Here we carry out a controlled approach, using DMRG-computed natural orbital bands, to downfold the three-band Hubbard model to an effective single band model. A sharp drop-off in the natural orbital occupancy at the edge of the first band provides a clear justification for a single-band model. Constructing Wannier functions from the first band, we compute all possible two-particle terms and retain those with significant magnitude. The resulting single-band model includes two-site occupancy-dependent hopping terms with $t_n \sim 0.6t$. These terms lead to a reduction of the ratio U/t_{eff} , and are important in capturing the doping-asymmetric carrier mobility, as well as in enhancing the pairing in a single-band model for the hole-doped cuprates. A measurement of the superconducting phase stiffness reveals that a mean-field treatment of the new terms is not nearly as effective in enhancing pairing as the terms themselves.

Introduction.— What is the minimal model that captures the important physics of the high-temperature cuprate superconductors? This has been a central question ever since the discovery of the cuprates. It has been argued that the single-band Hubbard and t - J model, in their simplest forms, are sufficient to describe the physics of high T_c superconductivity. Unexpectedly, recent numerical simulations find that superconductivity in these single-band models appears to be quite delicate. For example, in the purely nearest-neighbor hopping Hubbard model ($t', t'' = 0$), superconductivity is found to be absent [1]. Furthermore, in the extended t - J models (t' or $t'' \neq 0$), superconductivity is not present on the hole-doped side [2–4]. The greatest delicacy appears to be associated with the superconductivity; other aspects of the models, including antiferromagnetism (AFM) as well as the presence of intertwined spin and charge order, appear to be in qualitative agreement with the cuprates [2, 3, 5–10].

This subtlety of pairing in the single-band models calls for a re-examination of the downfolding process used to derive them, since modest errors could have significant effects. This downfolding is a two-step process, where first one constructs from density functional methods the intermediate-level three-band Hubbard (or Emery) model [11], which includes Cu $d_{x^2-y^2}$, O p_x and O p_y orbitals. Since the three-band model is closer to an all-electron Hamiltonian of the cuprates, one expects it to be more reliable than a one-band model—but also more difficult to simulate. There is evidence that the three-band model captures various aspects of the cuprates, particularly magnetic and charge density wave properties [12–19], with greater uncertainty about the pairing properties. To downfold to a single band model, Zhang and Rice argued that holes on oxygen sites bind to holes on copper sites to form local singlets [20]. The Zhang-Rice

singlet picture has gained support from experiments [21–23] as well as calculations [13, 14, 24, 25], and motivated studies of various single-band Hubbard [26–45] and t - J models [46–54].

Here we demonstrate an alternative way to downfold the three-band Hubbard model based on a density-matrix renormalization group (DMRG) [55] construction of Cu-centered Wannier functions. The general idea of constructing effective models using *ab initio* calculations has been explored in various contexts [56–60]. Our approach uses DMRG to compute the natural orbitals of the three-band model, and from those construct Wannier functions, similar to a recent work that downfolds hydrogen chains into Hubbard-like models [61]. The resulting single-band model includes additional two-site occupancy-dependent hopping terms t_n whose magnitude is comparable to t . On a mean-field level, these new terms simply reduce the ratio U/t_{eff} . However, beyond mean-field, the t_n terms capture the doping-asymmetric carrier mobility, and, as revealed by a measurement of the superconducting phase stiffness, further enhance the pairing in the hole-doped single-band model.

The three-band model.—We present the lattice structure and the terms in the three-band Hubbard model in Fig. 1(a). Each CuO_2 unit cell consists of three orbitals: Cu $d_{x^2-y^2}$, O p_x and O p_y . In the undoped insulator at half-filling, there is one hole per unit cell, and the model is written in the hole picture with $d_{i\sigma}^\dagger$ or $p_{j\sigma}^\dagger$ creating a hole with spin σ on a Cu site i or O site j . Hole doping corresponds to $n > 1$ while electron doping corresponds to $n < 1$. The three-band Hamiltonian is:

$$\begin{aligned}
 H^{TB} = & -t_{pd} \sum_{\langle ij \rangle \sigma} (d_{i\sigma}^\dagger p_{j\sigma} + h.c.) - t_{pp} \sum_{\langle ij \rangle \sigma} (p_{i\sigma}^\dagger p_{j\sigma} + h.c.) \\
 & + U_d \sum_i n_{i\uparrow}^d n_{i\downarrow}^d + U_p \sum_i n_{i\uparrow}^p n_{i\downarrow}^p + \Delta_{pd} \sum_{i\sigma} p_{i\sigma}^\dagger p_{i\sigma}
 \end{aligned} \tag{1}$$

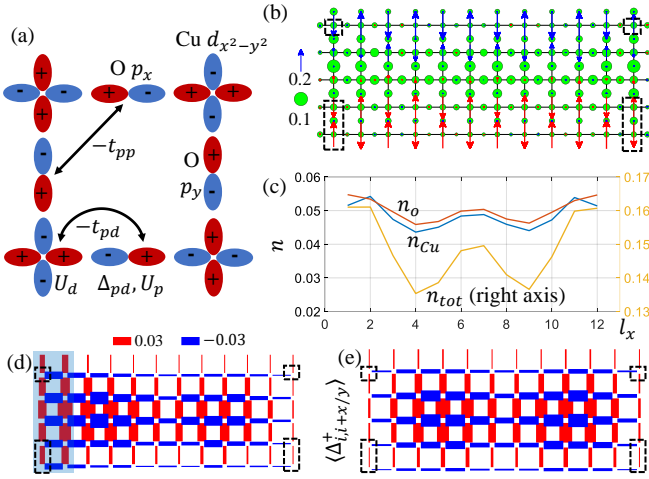


FIG. 1. (a): The three-band Hubbard model and our phase convention for the orbital basis. (b): Charge and spin structure on a 12×5 cylinder at a hole doping ~ 0.15 . The length of the arrows and the diameter of the circles represent $\langle S^z \rangle$ and local doping, respectively. The spins are colored to indicate different AFM domains. There are weak magnetic pinning fields applied on the boundary sites in the dotted boxes. (c): Average orbital-resolved local doping n along the length of the cylinder. (e) and (f): Pairing order $\langle \Delta_{ij}^\dagger + \Delta_{ij} \rangle$ between neighboring Cu sites i and j . The thickness/color of the bond indicates the magnitude/sign of the pairing. The pairing orders away from the edges are similar for (f) which has pairfields applied on the shaded left edge and (e) which spontaneously breaks symmetry.

where t_{pd}/t_{pp} hops a hole between nearest-neighbor Cu-O/O-O sites, and the summation $\langle ij \rangle$ runs over all relevant pairs of sites. We have chosen a gauge so that all hoppings are negative; U_d and U_p are the on-site repulsion term on Cu and O sites; $\Delta_{pd} = \epsilon_p - \epsilon_d$ is the energy difference for occupying an O site compared to occupying a Cu site. Unless otherwise noted, the parameters we use are: $t_{pd} = 1.0$, $t_{pp} = 0.5$, $U_d = 6.0$, $U_p = 3.0$, and $\Delta_{pd} = 3.5$, which appropriately describes a charge-transfer system where $U_d > \Delta_{pd}$ and $\Delta_{pd} > 2t_{pd}$. Comparing with previously used parameters [16, 62], here we increase Δ_{pd} to incorporate the effect of V_{pd} , and choose a somewhat smaller U_d for a stronger pairing response [63]. The calculations are carried out using the ITensor library [64]. We typically perform around 20 sweeps and keep a maximum bond dimension of 5000 to ensure convergence with a maximum truncation error of $\mathcal{O}(10^{-5})$.

Previous studies of the three-band model have identified features consistent with the cuprates, including doping asymmetry, formation of stripes on the hole doped side and commensurate AFM on the electron-doped side [15, 16]. There is evidence for d -wave pairing for both electron and hole doping, with the dominant component between nearest neighbor Cu sites [13, 14, 18, 65, 66].

Of particular concern for finite size effects is the quantization of stripe filling around a short cylinder [16]; here we choose a width-5 cylinder so that one stripe can form

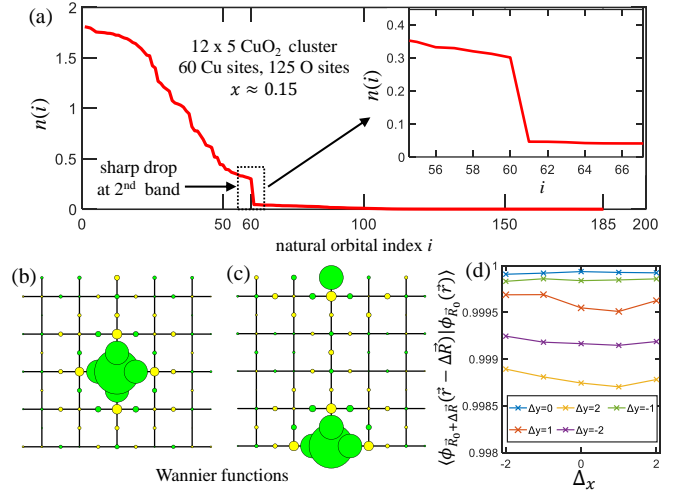


FIG. 2. At a hole doping of 0.15 (a): occupancies of the natural orbitals obtained by diagonalizing the single-particle correlation matrix $M_{\alpha\beta} = \sum_{\sigma} \langle C_{\alpha\sigma}^\dagger C_{\beta\sigma} \rangle$, with $C^\dagger = \{d, p_x^\dagger, p_y^\dagger\}$. The natural orbital states/occupancies correspond to the eigenvectors/eigenvalues of $M_{\alpha\beta}$. The inset is a zoom-in of the region that shows a sharp drop at the second band beyond which occupancies are limited ($< 2\%$). (b) and (c): cu-centered Wannier functions at two different locations constructed from the natural orbitals of the first band. Color/area of the circles indicate the sign/magnitude of the local orbital component. (e): overlap of Wannier functions (truncated to a 5×5 CuO_2 unit cell) with their centers shifted to the same site, showing they are almost translational invariant.

lengthwise; see Fig. 1(b). The Cu-Cu pairing is shown in Fig. 1(e). Along the stripe an additional pairing modulation reflects an edge-induced charge density oscillation, as shown in Fig. 1(c). Similar pairing occurs whether it is pinned by edge pair fields [Fig. 1(d)] or allowed to arise spontaneously as a finite bond dimension broken symmetry [2] [Fig. 1(e)].

Downfolding into a Wannier single-band model.—The occupied bands are identified from the DMRG measurement of the single-particle correlation matrix $M_{\alpha\beta} = \sum_{\sigma} \langle C_{\alpha\sigma}^\dagger C_{\beta\sigma} \rangle$, with $C^\dagger = \{d, p_x^\dagger, p_y^\dagger\}$, whose eigenvectors are the natural orbitals (NOs). In a non-interacting system, the NO eigenvalues (occupancies) make a step function at the Fermi level. Here, this step near $i \sim 35$ is completely smeared out [Fig. 2(a)], but another step occurs as $i = 60$, the number of Cu sites. Beyond this first band, the total occupancy is $< 2\%$, and for the electron doped case, $< 0.4\%$. This provides a strong justification for single-band downfolding, which would be exact if higher-band occupancies were zero.

Next, we localize the first NO band to construct Wannier functions (WFs), each localized around a Cu site; see Ref. [63] for details. We show two representative WF in Fig. 2(b) and (c), which are almost the same except for translation. Evidence of this translational invariance away from edges is shown in Fig. 2(d).

The one and two particle parts (1p and 2p) of the three

TABLE I. Parameters for the Wannier single-band model ($t = 1$ as unit) from downfolding the three-band model with (U_d, Δ_{pd}, n) . Case **h(e)** corresponds to hole(electron) doping.

case (U_d, Δ_{pd}, n)	t_n	t'	t'_n	t''	t''_n	U
h1* (6.0, 3.5, 1.15)	0.60	0.07	0.05	-0.04	-0.09	12.6
e1 (6.0, 3.5, 0.85)	0.52	0.08	0.08	-0.05	-0.04	13.7
h2 (3.0, 8.0, 1.15)	0.16	0.10	0.03	-0.03	-0.02	12.4

*Used in the majority of the calculations.

band model are projected into the WF space via

$$H^W = \hat{P}H_{1p}^{\text{TB}}\hat{P}^\dagger + \hat{P}^{\otimes 2}H_{2p}^{\text{TB}}(\hat{P}^\dagger)^{\otimes 2}. \quad (2)$$

where the rows of matrix \hat{P} are the WFs. Although H^W has $\mathcal{O}(N^2)$ single particle and $\mathcal{O}(N^4)$ two particle terms, the terms decay quickly with the distance between sites. Magnitudes of single particle hopping beyond third-nearest are smaller than $0.005t$ and are truncated. All of the two-particle terms arise from transformations of the U_d and the U_p terms. The leading term is an onsite repulsion $Un_{i\uparrow}n_{i\downarrow}$. The next largest terms come from replacing one of the c_i^\dagger or c_i operators with $c_{i+\delta}^\dagger$ or $c_{i+\delta}$ on a different site. These form the density-dependent hopping terms $t_n^\delta(c_{i+\delta,\sigma}^\dagger c_{i,\sigma})n_{i\bar{\sigma}}$, which have significant magnitudes because of the large value of U_d . We truncate the t_n^δ terms with δ beyond third-nearest neighbor, which are all smaller than $0.05t$. Terms at a greater distance cannot be generated reliably from the width-5 three-band cylinder. Higher-order two-particle terms involve multiple such replacements and are of $\mathcal{O}(t_n^2/U \sim 0.03t)$, which we neglect. After these simplifications, we obtain a *truncated Wannier model*:

$$H = \sum_{i,\delta,\sigma} -t^\delta c_{i+\delta,\sigma}^\dagger c_{i,\sigma} + \sum_i Un_{i\uparrow}n_{i\downarrow} + \sum_{i,\delta,\sigma} -t_n^\delta (c_{i+\delta,\sigma}^\dagger c_{i,\sigma} + c_{i,\sigma}^\dagger c_{i+\delta,\sigma})n_{i\bar{\sigma}}. \quad (3)$$

Here $i + \delta$ is the first, second, or third nearest neighbor of site i , with conventional hopping amplitudes t , t' , and t'' , and with occupancy-dependent hopping amplitudes t_n , t'_n , t''_n . The resulting model parameters are summarized in Table. I for downfolding based on three different three-band systems. Note that the WFs and thus the model parameters are similar for the hole and electron doped cases. The hopping coefficients are averaged over horizontal and vertical directions, which typically differ by $\sim 10\%$, but somewhat more (-0.07 and -0.11) in the case of t''_n in system **h1**.

The near-neighbor t_n coefficients are almost twice the size of an effective exchange coupling $J \sim 4t^2/U \sim 0.32$. The larger t_n in the cuprate-relevant charge transfer case (**h1**, **e1**), where double occupancy in a unit cell involves occupying a neighboring O-site, is directly tied to the

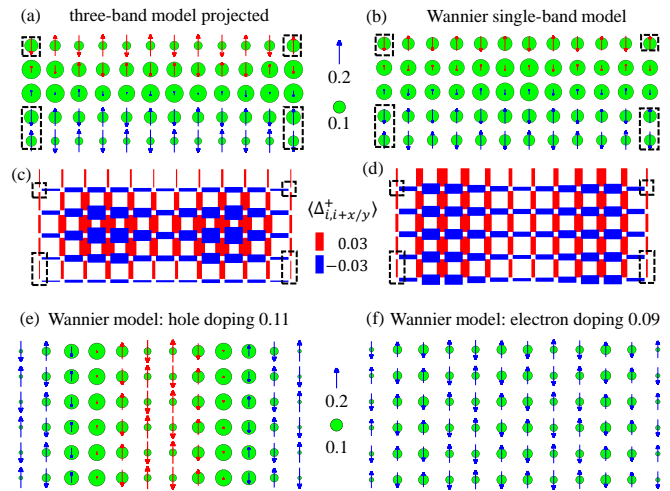


FIG. 3. (a) Spin and charge measurements for the ground state of the three-band model projected into the single band space defined by the Wannier functions, comparing to (b), direct simulation of the same quantities in the truncated Wannier model defined by Eq. 3. (c) and (d): for the same two systems, the pairing order $\langle \Delta_{ij}^\dagger + \Delta_{ij} \rangle$ between neighboring sites i and j is shown. Panels (e) and (f) show simulations of the truncated Wannier model on width-6 cylinders for hole doping of 0.12 and electron doping of 0.09, respectively. The stripes in (e) and the nearly uniform antiferromagnetism in (f) match the expected behavior from previous model studies as well as the cuprates.

higher O-occupancy in the WFs. Given their magnitude, it is surprising how rarely these terms have been considered [67–70].

In Fig. 3 we check H by comparing its ground-state properties to those of the original three-band model projected into the Wannier basis. Apart from minor differences in the amplitude of the hole density and the pairing modulation along the y direction, the effective single-band model manages to capture the local charge and spin order, the single-particle correlations (see Ref. [63]), and the pairing order. Simulations of H on a width-6 cylinder for both hole and electron doping are presented in Fig. 3 (e) and (f). The occurrence of stripes (hole doping) and commensurate AFM (electron doping) is consistent with the three-band model [16] as well as the cuprates. To study the more difficult pairing properties we turn to width-4 cylinders.

Effects of t_n —We find that the t_n terms have two primary effects: first, they reduce the effective interaction strength U/t_{eff} ; and second, they enhance hole hopping, reducing the effective mass of pairs on the hole-doped side and promoting phase coherence. The reduction of U/t_{eff} can be understood from a mean-field treatment of t_n where one replaces $t_n c_{j\sigma}^\dagger c_{i\sigma} (n_{i\bar{\sigma}} + n_{j\bar{\sigma}})$ by $t_n c_{j\sigma}^\dagger c_{i\sigma} \langle n \rangle$, with $\langle n \rangle$ being the average density of the system, adding to the conventional hopping. This changes $U/t \sim 13$ to $U/t_{\text{eff}} \sim 7.5$ (for $t_n=0.6$, $n=1.15$), close to $U/t = 8$, which is often used for the cuprates.

Beyond mean-field, we consider specific hopping pro-

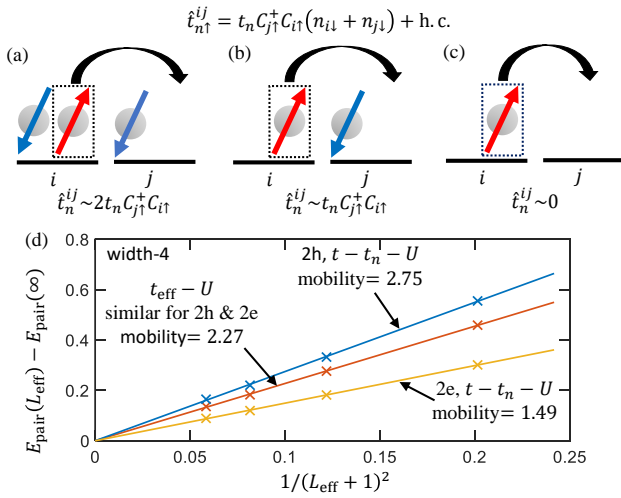


FIG. 4. (a),(b) and (c): action of the t_n term, and resulting hopping strengths, depending on the occupations of the sites involved. (d) On a width-4 cylinder, mobility of a pair of holes/electrons measured by the slope of pair energy versus $1/(L_{\text{eff}} + 1)^2$, for the t - t_n - U model and the t_{eff} - U model.

cesses in Fig. 4(a-c), written in the hole-picture. For a doped hole (i.e. a doublon) we expect process (a) to be relevant, where the t_n acts with magnitude $2t_n$. For undoped regions with AF particle-hole virtual hoppings, process (b) acts with magnitude t_n . On the electron doped side, process (c), t_n has no effect. It does not seem possible to capture these various properties correctly with a mean field treatment.

To measure pair effective mass, we consider a width-4 cylinder with either a hole-pair or electron-pair, and measure the pair kinetic energy through the changes in total energy with cylinder length [71], Fig. 4(d). To isolate the effects of t_n , we simulate a simplified the t - t_n - U model. The resulting hole-pair mobility is enhanced with the t_n term versus its mean-field, $2.75t$ versus $2.27t$. In contrast, the mobility of a pair of electrons with t_n is much smaller, $1.49t$, and reduced comparing to its mean-field $2.27t$.

To measure pairing directly and quantitatively, we measure the superconducting phase stiffness, as shown in Fig. 5. Here the applied fields allow us to estimate the phase stiffness via an energy difference, $\alpha \propto \frac{L_x}{\pi^2 L_y} \Delta E$, where ΔE can be extrapolated in the DMRG truncation error. At a hole doping of 0.11 ($n \approx 1.11$), the t - t_n - U model gives $\Delta E = 0.016(5)t$, significant pairing, whereas the t_{eff} pure Hubbard model has $\Delta E = 0.003(4)t$, consistent with the finding that the pure Hubbard model is non-superconducting [1]. Varying t_n in the supplementary material [63], we find that it always generates a bigger superconducting phase stiffness compared to its mean-field t_{eff} for a system with hole doping ~ 0.1 . In a more realistic model where t' and t'_n from Table. I are included, we find for a system with hole doping of 0.11 , $\Delta E = 0.012(4)$ with t_n versus $0.002(4)$ with t_{eff} . In contrast, for the electron doped system, ΔE is reduced with

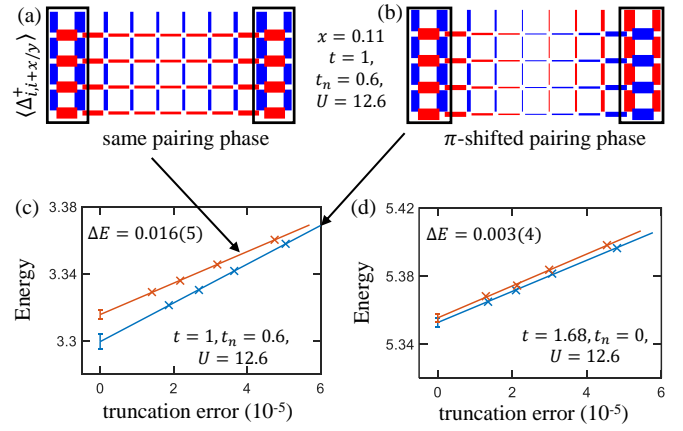


FIG. 5. Pairing response for the t - t_n - U model in a 10×4 cylinder at a hole doping ~ 0.11 ($n \approx 1.11$). Pair-fields have been applied to regions near both edges, denoted by the black boxes, with the phases on the two ends (a) being the same and (b) having a π shift. (c): extrapolated energies for the two different pairfield boundary conditions in (a) and (b). The energy difference is a measurement of the superconducting phase stiffness. (d) Same as (c) for the t_{eff} - U model that incorporates the effect of the t_n term only in mean-field.

t_n , $0.044(4)$, versus $0.068(5)$, at a doping of 0.09 .

Summary and discussion.— We have revisited the Zhang-Rice downfolding of the three-band Hubbard model to a single-band model, basing the downfolding on a DMRG simulation of the three band model. Our results give strong support to the applicability of the one band approach, where the small occupancy of higher natural orbital bands shows their irrelevance. However, our Wannier function downfolding then shows that a density dependent hopping term which is almost always neglected has a very large coefficient. This term renormalizes the hopping in mean field, but mean field treatments are inadequate to capture the effects of this term on pairing. The density dependent hopping enhances hole mobility and hole-pair mobility. This leads to enhanced superconducting pairing on the hole-doped side.

Recent simulations of the t - t' - U Hubbard model, combining AFQMC and DMRG and extrapolating to the thermodynamic limit, find that the hole-doped Hubbard model is superconducting [72]. However, the extrapolations are delicate, and it seems that this system must be close to the boundary between pairing and non-pairing phases. The addition of a t_n term may push the model well into the pairing regime, both easing the difficulties of simulating the model, and improving its applicability to the cuprates.

Acknowledgments.— We acknowledge helpful discussion with A. Georges, H.-C. Jiang and S. Sondhi. SJ and SRW are supported by the NSF under DMR-2110041.

* shengtaj@uci.edu

- [1] M. Qin, C.-M. Chung, H. Shi, E. Vitali, C. Hubig, U. Schollwöck, S. R. White, and S. Zhang (Simons Collaboration on the Many-Electron Problem), Absence of superconductivity in the pure two-dimensional Hubbard model, *Phys. Rev. X* **10**, 031016 (2020).
- [2] S. Jiang, D. J. Scalapino, and S. R. White, Ground-state phase diagram of the t - t' - J model, *Proc. Natl. Acad. Sci. U.S.A.* **118** (2021).
- [3] S. Jiang, D. J. Scalapino, and S. R. White, Pairing properties of the t - t' - J model, *Phys. Rev. B* **106**, 174507 (2022).
- [4] H.-C. Jiang and S. A. Kivelson, High temperature superconductivity in a lightly doped quantum spin liquid, *Phys. Rev. Lett.* **127**, 097002 (2021).
- [5] E. W. Huang, T. Liu, W. O. Wang, H.-C. Jiang, P. Mai, T. A. Maier, S. Johnston, B. Moritz, and T. P. Devereaux, Fluctuating intertwined stripes in the strange metal regime of the Hubbard model, *arXiv:2202.08845* (2022).
- [6] P. Mai, S. Karakuzu, G. Balduzzi, S. Johnston, and T. A. Maier, Intertwined spin, charge, and pair correlations in the two-dimensional Hubbard model in the thermodynamic limit, *Proc. Natl. Acad. Sci. U.S.A.* **119**, e2112806119 (2022).
- [7] M. Qin, T. Schäfer, S. Andergassen, P. Corboz, and E. Gull, The Hubbard model: A Computational Perspective, *Annu. Rev. Condens. Matter Phys.* **13**, 275 (2022).
- [8] W. He, J. Wen, H.-C. Jiang, G. Xu, W. Tian, T. Taniguchi, Y. Ikeda, M. Fujita, and Y. S. Lee, Prevalence of tilted stripes in $\text{La}_{1.88}\text{Sr}_{0.12}\text{CuO}_4$ and the importance of t' in the Hamiltonian, *arXiv:2107.10264* (2021).
- [9] E. W. Huang, C. B. Mendl, H.-C. Jiang, B. Moritz, and T. P. Devereaux, Stripe order from the perspective of the Hubbard model, *npj Quantum Mater.* **3**, 1 (2018).
- [10] S. Karakuzu, A. Tanjaron Ly, P. Mai, J. Neuhaus, T. A. Maier, and S. Johnston, Stripe correlations in the two-dimensional Hubbard-Holstein model, *Commun. Phys.* **5**, 1 (2022).
- [11] V. J. Emery, Theory of high- T_c superconductivity in oxides, *Phys. Rev. Lett.* **58**, 2794 (1987).
- [12] E. W. Huang, C. B. Mendl, S. Liu, S. Johnston, H.-C. Jiang, B. Moritz, and T. P. Devereaux, Numerical evidence of fluctuating stripes in the normal state of high- T_c cuprate superconductors, *Science* **358**, 1161 (2017).
- [13] P. Mai, G. Balduzzi, S. Johnston, and T. A. Maier, Orbital structure of the effective pairing interaction in the high-temperature superconducting cuprates, *npj Quantum Mater.* **6**, 1 (2021).
- [14] Z.-H. Cui, C. Sun, U. Ray, B.-X. Zheng, Q. Sun, and G. K.-L. Chan, Ground-state phase diagram of the three-band Hubbard model from density matrix embedding theory, *Phys. Rev. Res.* **2**, 043259 (2020).
- [15] A. Chiciak, E. Vitali, and S. Zhang, Magnetic and charge orders in the ground state of the emery model: Accurate numerical results, *Phys. Rev. B* **102**, 214512 (2020).
- [16] S. R. White and D. J. Scalapino, Doping asymmetry and striping in a three-orbital CuO_2 Hubbard model, *Phys. Rev. B* **92**, 205112 (2015).
- [17] N. Kowalski, S. S. Dash, P. Sémon, D. Sénéchal, and A.-M. Tremblay, Oxygen hole content, charge-transfer gap, covalency, and cuprate superconductivity, *Proc. Natl. Acad. Sci. U.S.A.* **118**, e2106476118 (2021).
- [18] A. Biborski, M. Zegrodnik, and J. Spałek, Superconducting properties of the hole-doped three-band $d - p$ model studied with minimal-size real-space d -wave pairing operators, *Phys. Rev. B* **101**, 214504 (2020).
- [19] S. Li, A. Nocera, U. Kumar, and S. Johnston, Particle-hole asymmetry in the dynamical spin and charge responses of corner-shared 1d cuprates, *Commun. Phys.* **4**, 217 (2021).
- [20] F. C. Zhang and T. M. Rice, Effective hamiltonian for the superconducting Cu oxides, *Phys. Rev. B* **37**, 3759 (1988).
- [21] N. B. Brookes, G. Ghiringhelli, O. Tjernberg, L. H. Tjeng, T. Mizokawa, T. W. Li, and A. A. Menovsky, Detection of Zhang-Rice Singlets Using Spin-Polarized Photoemission, *Phys. Rev. Lett.* **87**, 237003 (2001).
- [22] L. H. Tjeng, B. Sinkovic, N. B. Brookes, J. B. Goedkoop, R. Hesper, E. Pellegrin, F. M. F. de Groot, S. Altieri, S. L. Hulbert, E. Shekel, and G. A. Sawatzky, Spin-resolved photoemission on anti-ferromagnets: Direct observation of Zhang-Rice singlets in CuO, *Phys. Rev. Lett.* **78**, 1126 (1997).
- [23] Y. Harada, K. Okada, R. Eguchi, A. Kotani, H. Takagi, T. Takeuchi, and S. Shin, Unique identification of Zhang-Rice singlet excitation in $\text{Sr}_2\text{CuO}_2\text{Cl}_2$ mediated by the O 1s core hole: Symmetry-selective resonant soft x-ray Raman scattering study, *Phys. Rev. B* **66**, 165104 (2002).
- [24] E. Arrighoni, M. Aichhorn, M. Daghofer, and W. Hanke, Phase diagram and single-particle spectrum of CuO high- T_c layers: variational cluster approach to the three-band Hubbard model, *New J. Phys.* **11**, 055066 (2009).
- [25] I. J. Hamad, L. O. Manuel, and A. A. Aligia, Generalized one-band model based on Zhang-Rice singlets for tetragonal CuO, *Phys. Rev. Lett.* **120**, 177001 (2018).
- [26] V. Marino, F. Becca, and L. F. Tocchio, Stripes in the extended $t - t'$ Hubbard model: A Variational Monte Carlo analysis, *SciPost Phys.* **12**, 180 (2022).
- [27] Y.-F. Jiang, J. Zaanen, T. P. Devereaux, and H.-C. Jiang, Ground state phase diagram of the doped Hubbard model on the four-leg cylinder, *Phys. Rev. Research* **2**, 033073 (2020).
- [28] K. Ido, T. Ohgoe, and M. Imada, Competition among various charge-inhomogeneous states and d -wave superconducting state in Hubbard models on square lattices, *Phys. Rev. B* **97**, 045138 (2018).
- [29] L. F. Tocchio, F. Becca, and S. Sorella, Hidden Mott transition and large- U superconductivity in the two-dimensional Hubbard model, *Phys. Rev. B* **94**, 195126 (2016).
- [30] S. Sorella, The phase diagram of the Hubbard model by variational auxiliary field quantum monte carlo (2021), *arXiv:2101.07045*.
- [31] K. Ido, T. Ohgoe, and M. Imada, Competition among various charge-inhomogeneous states and d -wave superconducting state in Hubbard models on square lattices, *Phys. Rev. B* **97**, 045138 (2018).
- [32] L. F. Tocchio, A. Montorsi, and F. Becca, Metallic and insulating stripes and their relation with superconductivity in the doped Hubbard model, *SciPost Phys.* **7**, 21 (2019).
- [33] D. Sénéchal, P.-L. Lavertu, M.-A. Marois, and A.-M. S. Tremblay, Competition between antiferromagnetism and superconductivity in high- T_c cuprates, *Phys. Rev. Lett.* **94**, 156404 (2005).
- [34] K. Machida, Magnetism in La_2CuO_4 based compounds, *Physica C Supercond.* **158**, 192 (1989).
- [35] X. Y. Xu and T. Grover, Competing nodal d -wave super-

- conductivity and antiferromagnetism, Phys. Rev. Lett. **126**, 217002 (2021).
- [36] A. Himeda, T. Kato, and M. Ogata, Stripe states with spatially oscillating d -wave superconductivity in the two-dimensional $t-t'-J$ model, Phys. Rev. Lett. **88**, 117001 (2002).
- [37] H.-C. Jiang and S. A. Kivelson, Stripe order enhanced superconductivity in the hubbard model, Proc. Natl. Acad. Sci. U.S.A. **119**, e2109406119 (2022).
- [38] H. Xu, H. Shi, E. Vitali, M. Qin, and S. Zhang, Stripes and spin-density waves in the doped two-dimensional hubbard model: Ground state phase diagram, Phys. Rev. Res. **4**, 013239 (2022).
- [39] J. P. F. LeBlanc, A. E. Antipov, F. Becca, I. W. Bulik, G. K.-L. Chan, C.-M. Chung, Y. Deng, M. Ferrero, T. M. Henderson, C. A. Jiménez-Hoyos, E. Kozik, X.-W. Liu, A. J. Millis, N. V. Prokof'ev, M. Qin, G. E. Scuseria, H. Shi, B. V. Svistunov, L. F. Tocchio, I. S. Tupitsyn, S. R. White, S. Zhang, B.-X. Zheng, Z. Zhu, and E. Gull (Simons Collaboration on the Many-Electron Problem), Solutions of the two-dimensional Hubbard model: Benchmarks and results from a wide range of numerical algorithms, Phys. Rev. X **5**, 041041 (2015).
- [40] B.-X. Zheng, C.-M. Chung, P. Corboz, G. Ehlers, M.-P. Qin, R. M. Noack, H. Shi, S. R. White, S. Zhang, and G. K.-L. Chan, Stripe order in the underdoped region of the two-dimensional hubbard model, Science **358**, 1155 (2017).
- [41] C. Peng, Y. Wang, J. Wen, Y. Lee, T. Devereaux, and H.-C. Jiang, Enhanced superconductivity by near-neighbor attraction in the doped Hubbard model, arXiv:2206.03486 (2022).
- [42] A. Wietek, Y.-Y. He, S. R. White, A. Georges, and E. M. Stoudenmire, Stripes, antiferromagnetism, and the pseudogap in the doped Hubbard model at finite temperature, Phys. Rev. X **11**, 031007 (2021).
- [43] S. Raghu, S. A. Kivelson, and D. J. Scalapino, Superconductivity in the repulsive hubbard model: An asymptotically exact weak-coupling solution, Phys. Rev. B **81**, 224505 (2010).
- [44] B. Xiao, Y.-Y. He, A. Georges, and S. Zhang, Temperature dependence of spin and charge orders in the doped two-dimensional hubbard model, Phys. Rev. X **13**, 011007 (2023).
- [45] M. Danilov, E. G. van Loon, S. Brener, S. Isakov, M. I. Katsnelson, and A. I. Lichtenstein, Degenerate plaquette physics as key ingredient of high-temperature superconductivity in cuprates, npj Quantum Mater. **7**, 50 (2022).
- [46] P. Corboz, T. M. Rice, and M. Troyer, Competing states in the $t - J$ model: Uniform d -wave state versus stripe state, Phys. Rev. Lett. **113**, 046402 (2014).
- [47] H.-C. Jiang, Z.-Y. Weng, and S. A. Kivelson, Superconductivity in the doped $t - J$ model: Results for four-leg cylinders, Phys. Rev. B **98**, 140505(R) (2018).
- [48] J. F. Dodaro, H.-C. Jiang, and S. A. Kivelson, Intertwined order in a frustrated four-leg $t - J$ cylinder, Phys. Rev. B **95**, 155116 (2017).
- [49] P. Corboz, S. R. White, G. Vidal, and M. Troyer, Stripes in the two-dimensional $t-J$ model with infinite projected entangled-pair states, Phys. Rev. B **84**, 041108(R) (2011).
- [50] S. Gong, W. Zhu, and D. N. Sheng, Robust d -wave superconductivity in the square-lattice $t-J$ model, Phys. Rev. Lett. **127**, 097003 (2021).
- [51] C.-P. Chou and T.-K. Lee, Mechanism of formation of half-doped stripes in underdoped cuprates, Phys. Rev. B **81**, 060503(R) (2010).
- [52] W.-C. Chen, Y. Wang, and C.-C. Chen, Superconducting phases of the square-lattice extended hubbard model, arXiv:2206.01119 (2022).
- [53] D.-W. Qu, B.-B. Chen, X. Lu, Q. Li, Y. Qi, S.-S. Gong, W. Li, and G. Su, d -wave superconductivity, pseudogap, and the phase diagram of $t-t'-J$ model at finite temperature (2022).
- [54] H.-C. Jiang, S. A. Kivelson, and D.-H. Lee, Superconducting valence bond fluid in lightly doped 8-leg $t-J$ cylinders, arXiv:2302.11633 (2023).
- [55] S. R. White, Density matrix formulation for quantum renormalization groups, Phys. Rev. Lett. **69**, 2863 (1992).
- [56] Y. Chang and L. K. Wagner, Learning emergent models from *ab initio* many-body calculations, arXiv:2302.02899 (2023).
- [57] H. J. Changlani, H. Zheng, and L. K. Wagner, Density-matrix based determination of low-energy model hamiltonians from *ab initio* wavefunctions, J. Chem. Phys. **143**, 102814 (2015).
- [58] Z.-H. Cui, H. Zhai, X. Zhang, and G. K.-L. Chan, Systematic electronic structure in the cuprate parent state from quantum many-body simulations, Science **377**, 1192 (2022).
- [59] H. Zheng, H. J. Changlani, K. T. Williams, B. Busemeyer, and L. K. Wagner, From real materials to model hamiltonians with density matrix downfolding, Front. Phys. **6**, 10.3389/fphy.2018.00043 (2018).
- [60] M. Hirayama, Y. Nomura, and R. Arita, *Ab initio* downfolding based on the gw approximation for infinite-layer nickelates, Front. Phys. , 49 (2022).
- [61] R. C. Sawaya and S. R. White, Constructing hubbard models for the hydrogen chain using sliced-basis density matrix renormalization group, Phys. Rev. B **105**, 045145 (2022).
- [62] W. Hanke, M. L. Kiesel, M. Aichhorn, S. Brehm, and E. Arrighoni, The 3-band hubbard-model versus the 1-band model for the high- T_c cuprates: Pairing dynamics, superconductivity and the ground-state phase diagram, Eur. Phys. J.: Spec. Top. **188**, 15 (2010).
- [63] See Supplemental Material at [], which includes Refs. [14, 61, 62, 73], for details on pairing properties of the three-band Hubbard model, constructing Cu-centered Wannier functions, phase stiffness for varying t_n .
- [64] M. Fishman, S. R. White, and E. M. Stoudenmire, The ITensor Software Library for Tensor Network Calculations, SciPost Phys. Codebases , 4 (2022).
- [65] H.-C. Jiang, Pair density wave in doped three-band hubbard model on square lattice, arXiv:2209.11381 (2022).
- [66] J.-P. Song, S. Mazumdar, and R. T. Clay, Absence of Luther-Emery superconducting phase in the three-band model for cuprate ladders, Phys. Rev. B **104**, 104504 (2021).
- [67] F. Werner, O. Parcollet, A. Georges, and S. R. Hassan, Interaction-induced adiabatic cooling and antiferromagnetism of cold fermions in optical lattices, Phys. Rev. Lett. **95**, 056401 (2005).
- [68] J. Hirsch, Bond-charge repulsion and hole superconductivity, Phys. C: Supercond. Appl. **158**, 326 (1989).
- [69] R. B. Laughlin, Fermi-liquid computation of the phase diagram of high- T_c cuprate superconductors with an orbital antiferromagnetic pseudogap, Phys. Rev. Lett. **112**,

- 017004 (2014).
- [70] S. L. Sondhi, M. P. Gelfand, H. Q. Lin, and D. K. Campbell, Off-diagonal interactions, Hund's rules, and pair binding in c_{60} , *Phys. Rev. B* **51**, 5943 (1995).
- [71] S. Daul, D. J. Scalapino, and S. R. White, Pairing correlations on $t - U - J$ ladders, *Phys. Rev. Lett.* **84**, 4188 (2000).
- [72] H. Xu, C.-M. Chung, M. Qin, U. Schollwöck, S. R. White, and S. Zhang, Coexistence of superconductivity with partially filled stripes in the Hubbard model, arXiv:2303.08376 (2023).
- [73] P.-O. Löwdin, On the non-orthogonality problem connected with the use of atomic wave functions in the theory of molecules and crystals, *J. Chem. Phys.* **18**, 365 (1950).

A single-band model with enhanced pairing from DMRG-based downfolding of the three-band Hubbard model: Supplemental Materials

Shengtao Jiang (蒋晨韬)^{1,*}, Douglas J. Scalapino,² and Steven R. White¹

¹Department of Physics and Astronomy, University of California, Irvine, California 92697, USA

²Department of Physics, University of California, Santa Barbara, California 93106, USA

(Dated: March 23, 2023)

I. PARAMETERS FOR THE THREE-BAND HUBBARD MODEL

A common choice of the parameters for the three-band Hubbard model is: $t_{pd} = 1.0$, $t_{pp} = 0.5$, $\Delta_{pd} = 3.0$, $U_{dd} = 8.0$, $U_{pp} = 3.0$, $V_{pd} = 0.5$ [1]. In a recent density-matrix embedding theory [2], the appropriate range of U_{dd} is estimated to be 4.5-9.3 when fixing other parameters as in the common choice. While the common choice $U_{dd} = 8.0$ falls in the upper half of this range, we also consider another $U_{dd} = 6.0$ in the lower half of this range. In addition, we omit V_{pd} but increase Δ_{pd} to 3.5 to incorporate its effect. A comparison of the pairing responses of these two choices of U_{dd} are shown in Fig. S1, and $U_{dd} = 6.0$ exhibits a stronger pairing response, so we choose it for a clearer signal.

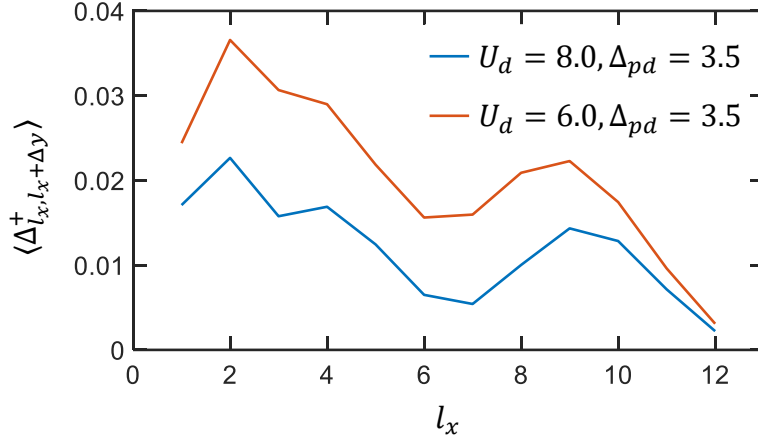


FIG. S1. Pairing response of two different U_{dd} with pairfields applied on two columns ($l_x = 1, 2$) on the left edge of a 12×5 cylinder, at a hole doping of 0.15 ($n = 1.15$). Both the applied pairfields and the pairing responses are on nearest-neighbor vertical Cu-Cu bonds.

II. FURTHER DETAILS ON WANNIER CONSTRUCTIONS AND THE RESULTING SINGLE-BAND MODEL

Our construction of the Wannier functions and subsequent downfolding is patterned after Ref. [3], with the key difference being that in our study we start with a three band model rather than a continuum all electron calculation described by sliced basis functions. The goal is to form Wannier functions centered at Cu site j $\{\phi_j(\vec{r})\}$ by linearly combining the natural orbitals of the first-band $\{\psi_i(\vec{r})\}$, with both i and j ranging from 1 to the total number of Cu sites. We would like the Wannier functions to be: (1) orthonormal, (2) translationally invariant, and (3) localized around Cu sites. These properties ensure the downfolded Wannier Hamiltonian has short-ranged interactions with site-independent magnitudes. While the translational invariance cannot be completely achieved because we are dealing with cylindrical systems with open edges, we expect the Wannier functions in the bulk to almost satisfy the above properties.

* shengtaj@uci.edu

First we construct functions $\{\delta_j(\vec{r})\}$ localized around each Cu site j by superposing the natural orbitals $\{\psi_i\}$ with coefficients being their respective weight on Cu site j :

$$\delta_j(\vec{r}) = \sum_i \psi_i(\vec{r} = \vec{r}_j) \psi_i(\vec{r}) \quad (1)$$

where \vec{r}_j is the position vector corresponding to Cu site j . The functions $\{\delta_j(\vec{r})\}$ are localized, but not orthonormal. We orthonormalize them while preserving their locality using Löwdin symmetric orthogonalization [4], which minimally rotates these functions (note O is a matrix):

$$\begin{aligned} \phi_j(\vec{r}) &= \sum_{j'} [O^{-\frac{1}{2}}]_{jj'} \delta_{j'}(\vec{r}), \\ \text{with } O_{jj'} &= \langle \delta_j(\vec{r}) | \delta_{j'}(\vec{r}) \rangle. \end{aligned} \quad (2)$$

The resulting Wannier functions $\{\phi_j(\vec{r})\}$ are guaranteed to be orthonormal and are almost translational invariant, as we show in Fig. 2(e) in the main text. We plot the structure of the resulting Wannier function in the figure below. It is localized around one Cu site with its tail decaying rapidly with the distance away from the center Cu site. Due to the width-5 cylinder used, there are differences between the coefficient of orbitals in vertical and horizontal directions at long distance. While we do not further modify the Wannier functions, so as to preserve orthonormality, we do later average the terms over the two directions in the downfolded Hamiltonian.

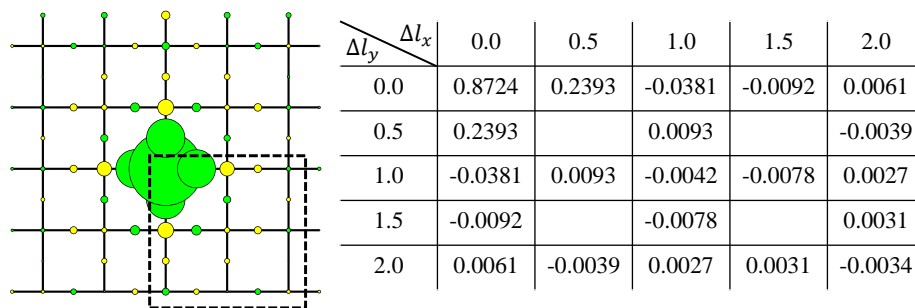


FIG. S2. A Cu-centered Wannier function with the color/area of the circles denoting the sign/magnitude of the local orbital components. The coefficients of the orbitals in the lower-right quadrant are shown in the table, which have been averaged over the vertical and horizontal directions.

After constructions of Wannier functions, we derive the downfolded single-band model by projecting the three-band Hamiltonian on the Wannier basis and truncate terms with small magnitude. The validity of the downfolded model is verified by the consistency in the local spin and charge order and pairing order with the original three-band model (shown in the main text), as well as the single-particle correlation presented below in Fig. S3.

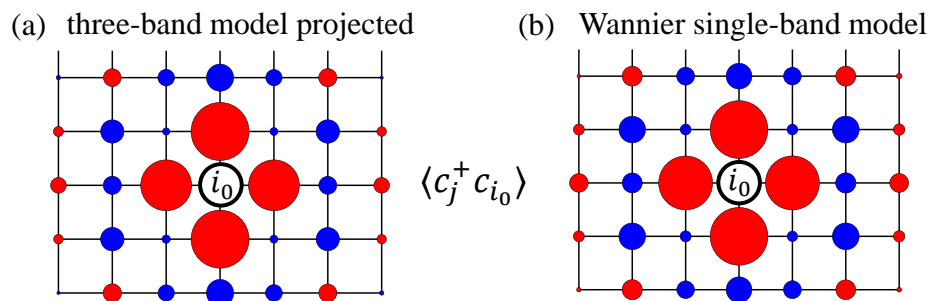


FIG. S3. Single-particle correlation function for (a) the three-band model projected into the Wannier basis and (b) the truncated Wannier single-band model. The area/color of the circle on site j indicate the magnitude/sign of the correlation $\sum_\sigma \langle C_{j\sigma}^\dagger C_{i_0\sigma} \rangle$ with i_0 being the center reference site.

The biggest difference between the Wannier single-band model with the conventional model is the additional doping-dependent hopping term $t_n \sim 0.6t$, which further enhances pairing comparing to its mean-field. In Fig. S4 below, we vary the magnitude of t_n and find that it always produces a bigger superconducting phase stiffness, compared with the mean-field treatment where the t_n term is incorporated into the ordinary hopping t_{eff} .

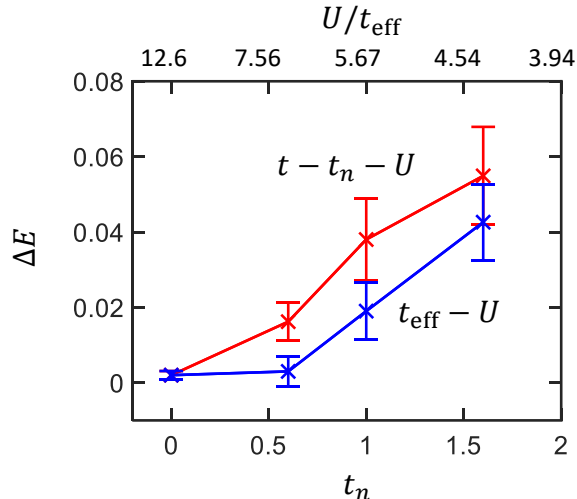


FIG. S4. Superconducting phase stiffness reflected by the energy difference for different pairfield boundary conditions (see the main text) as a function of t_n and corresponding mean-field t_{eff} . $t = 1$ is the energy unit and $U = 12.6$ for both models.

-
- [1] W. Hanke, M. L. Kiesel, M. Aichhorn, S. Brehm, and E. Arrighoni, The 3-band hubbard-model versus the 1-band model for the high- t c cuprates: Pairing dynamics, superconductivity and the ground-state phase diagram, *Eur. Phys. J.: Spec. Top.* **188**, 15 (2010).
 - [2] Z.-H. Cui, C. Sun, U. Ray, B.-X. Zheng, Q. Sun, and G. K.-L. Chan, Ground-state phase diagram of the three-band hubbard model from density matrix embedding theory, *Phys. Rev. Res.* **2**, 043259 (2020).
 - [3] R. C. Sawaya and S. R. White, Constructing hubbard models for the hydrogen chain using sliced-basis density matrix renormalization group, *Phys. Rev. B* **105**, 045145 (2022).
 - [4] P.-O. Löwdin, On the non-orthogonality problem connected with the use of atomic wave functions in the theory of molecules and crystals, *J. Chem. Phys.* **18**, 365 (1950).